

Atmospheric effects on extensive air showers observed with the Surface Detector of the Pierre Auger Observatory

The Pierre Auger Collaboration

J. Abraham⁸, P. Abreu⁷¹, M. Aglietta⁵⁴, C. Aguirre¹², E.J. Ahn⁸⁷,
D. Allard³¹, I. Allekotte¹, J. Allen⁹⁰, P. Allison⁹², J. Alvarez-Muñiz⁷⁸,
M. Ambrosio⁴⁸, L. Anchordoqui¹⁰⁴, S. Andringa⁷¹, A. Anzalone⁵³,
C. Aramo⁴⁸, E. Arganda⁷⁵, S. Argirò⁵¹, K. Arisaka⁹⁵, F. Arneodo⁵⁵,
F. Arqueros⁷⁵, T. Asch³⁸, H. Asorey¹, P. Assis⁷¹, J. Aublin³³, M. Ave⁹⁶,
G. Avila¹⁰, T. Bäckér⁴², D. Badagnani⁶, K.B. Barber¹¹, A.F. Barbosa¹⁴,
S.L.C. Barroso²⁰, B. Baughman⁹², P. Bauleo⁸⁵, J.J. Beatty⁹², T. Beau³¹,
B.R. Becker¹⁰¹, K.H. Becker³⁶, A. Bellétoile³⁴, J.A. Bellido^{11, 93}, S. BenZvi¹⁰³,
C. Berat³⁴, P. Bernardini⁴⁷, X. Bertou¹, P.L. Biermann³⁹, P. Billoir³³,
O. Blanch-Bigas³³, F. Blanco⁷⁵, C. Bleve⁴⁷, H. Blümer^{41, 37},
M. Boháčová^{96, 27}, C. Bonifazi³³, R. Bonino⁵⁴, N. Borodai⁶⁹, J. Brack⁸⁵,
P. Brogueira⁷¹, W.C. Brown⁸⁶, R. Bruijn⁸¹, P. Buchholz⁴², A. Bueno⁷⁷,
R.E. Burton⁸³, N.G. Busca³¹, K.S. Caballero-Mora⁴¹, L. Caramete³⁹,
R. Caruso⁵⁰, W. Carvalho¹⁷, A. Castellina⁵⁴, O. Catalano⁵³, L. Cazon⁹⁶,
R. Cester⁵¹, J. Chauvin³⁴, A. Chiavassa⁵⁴, J.A. Chinellato¹⁸, A. Chou^{87, 90},
J. Chudoba²⁷, J. Chye⁸⁹, R.W. Clay¹¹, E. Colombo², R. Conceição⁷¹,
B. Connolly¹⁰², F. Contreras⁹, J. Coppens^{65, 67}, A. Cordier³², U. Cotti⁶³,
S. Coutu⁹³, C.E. Covault⁸³, A. Creusot⁷³, A. Criss⁹³, J. Cronin⁹⁶,
A. Curutiu³⁹, S. Dagoret-Campagne³², R. Dallier³⁵, K. Daumiller³⁷,
B.R. Dawson¹¹, R.M. de Almeida¹⁸, M. De Domenico⁵⁰, C. De Donato⁴⁶,
S.J. de Jong⁶⁵, G. De La Vega⁸, W.J.M. de Mello Junior¹⁸, J.R.T. de Mello
Neto²³, I. De Mitri⁴⁷, V. de Souza¹⁶, K.D. de Vries⁶⁶, G. Decerprit³¹, L. del
Peral⁷⁶, O. Deligny³⁰, A. Della Selva⁴⁸, C. Delle Fratte⁴⁹, H. Dembinski⁴⁰,
C. Di Giulio⁴⁹, J.C. Diaz⁸⁹, P.N. Diep¹⁰⁵, C. Dobrigkeit¹⁸, J.C. D'Olive⁶⁴,
P.N. Dong¹⁰⁵, D. Dornic³⁰, A. Dorofeev⁸⁸, J.C. dos Anjos¹⁴, M.T. Dova⁶,
D. D'Urso⁴⁸, I. Dutan³⁹, M.A. DuVernois⁹⁸, R. Engel³⁷, M. Erdmann⁴⁰,
C.O. Escobar¹⁸, A. Etchegoyen², P. Facal San Luis^{96, 78}, H. Falcke^{65, 68},
G. Farrar⁹⁰, A.C. Fauth¹⁸, N. Fazzini⁸⁷, F. Ferrer⁸³, A. Ferrero², B. Fick⁸⁹,
A. Filevich², A. Filipčič^{72, 73}, I. Fleck⁴², S. Fliescher⁴⁰, C.E. Fracchiolla¹⁵,
E.D. Fraenkel⁶⁶, W. Fulgione⁵⁴, R.F. Gamarra², S. Gambetta⁴⁴, B. García⁸,
D. García Gámez⁷⁷, D. Garcia-Pinto⁷⁵, X. Garrido^{37, 32}, G. Gelmini⁹⁵,
H. Gemmeke³⁸, P.L. Ghia^{30, 54}, U. Giaccari⁴⁷, M. Giller⁷⁰, H. Glass⁸⁷,
L.M. Goggin¹⁰⁴, M.S. Gold¹⁰¹, G. Golup¹, F. Gomez Albarracin⁶, M. Gómez
Berisso¹, P. Gonçalves⁷¹, M. Gonçalves do Amaral²⁴, D. Gonzalez⁴¹,
J.G. Gonzalez^{77, 88}, D. Góra^{41, 69}, A. Gorgi⁵⁴, P. Gouffon¹⁷, E. Grashorn⁹²,
S. Grebe⁶⁵, M. Grigat⁴⁰, A.F. Grillo⁵⁵, Y. Guardincerri⁴, F. Guarino⁴⁸,

G.P. Guedes¹⁹, J. Gutiérrez⁷⁶, J.D. Hague¹⁰¹, V. Halenka²⁸, P. Hansen⁶,
 D. Harari¹, S. Harmsma^{66, 67}, J.L. Harton⁸⁵, A. Haungs³⁷, M.D. Healy⁹⁵,
 T. Hebbeker⁴⁰, G. Hebrero⁷⁶, D. Heck³⁷, C. Hojvat⁸⁷, V.C. Holmes¹¹,
 P. Homola⁶⁹, J.R. Hörandel⁶⁵, A. Horneffer⁶⁵, M. Hrabovský^{28, 27},
 T. Huege³⁷, M. Hussain⁷³, M. Iarlori⁴⁵, A. Insolia⁵⁰, F. Ionita⁹⁶, A. Italiano⁵⁰,
 S. Jiraskova⁶⁵, M. Kaducak⁸⁷, K.H. Kampert³⁶, T. Karova²⁷, P. Kasper⁸⁷,
 B. Kégl³², B. Keilhauer³⁷, E. Kemp¹⁸, R.M. Kieckhafer⁸⁹, H.O. Klages³⁷,
 M. Kleifges³⁸, J. Kleinfeller³⁷, R. Knapik⁸⁵, J. Knapp⁸¹, D.-H. Koang³⁴,
 A. Krieger², O. Krömer³⁸, D. Kruppke-Hansen³⁶, D. Kuempel³⁶, N. Kunka³⁸,
 A. Kusenko⁹⁵, G. La Rosa⁵³, C. Lachaud³¹, B.L. Lago²³, P. Lautridou³⁵,
 M.S.A.B. Leão²², D. Lebrun³⁴, P. Lebrun⁸⁷, J. Lee⁹⁵, M.A. Leigui de
 Oliveira²², A. Lemiere³⁰, A. Letessier-Selvon³³, M. Leuthold⁴⁰,
 I. Lhenry-Yvon³⁰, R. López⁵⁹, A. Lopez Agüera⁷⁸, K. Louedec³², J. Lozano
 Bahilo⁷⁷, A. Lucero⁵⁴, R. Luna García⁶², H. Lyberis³⁰, M.C. Maccarone⁵³,
 C. Macolino⁴⁵, S. Maldera⁵⁴, D. Mandat²⁷, P. Mantsch⁸⁷, A.G. Mariazzi⁶,
 I.C. Maris⁴¹, H.R. Marquez Falcon⁶³, D. Martello⁴⁷, J. Martínez⁶²,
 O. Martínez Bravo⁵⁹, H.J. Mathes³⁷, J. Matthews^{88, 94}, J.A.J. Matthews¹⁰¹,
 G. Matthiae⁴⁹, D. Maurizio⁵¹, P.O. Mazur⁸⁷, M. McEwen⁷⁶, R.R. McNeil⁸⁸,
 G. Medina-Tanco⁶⁴, M. Melissas⁴¹, D. Melo⁵¹, E. Menichetti⁵¹,
 A. Menshikov³⁸, R. Meyhandan⁶⁶, M.I. Micheletti², G. Miele⁴⁸, W. Miller¹⁰¹,
 L. Miramonti⁴⁶, S. Mollerach¹, M. Monasor⁷⁵, D. Monnier Ragainne³²,
 F. Montanet³⁴, B. Morales⁶⁴, C. Morello⁵⁴, J.C. Moreno⁶, C. Morris⁹²,
 M. Mostafá⁸⁵, C.A. Moura⁴⁸, S. Mueller³⁷, M.A. Muller¹⁸, R. Mussa⁵¹,
 G. Navarra⁵⁴, J.L. Navarro⁷⁷, S. Navas⁷⁷, P. Necasal²⁷, L. Nellen⁶⁴,
 C. Newman-Holmes⁸⁷, D. Newton⁸¹, P.T. Nhung¹⁰⁵, N. Nierstenhoefer³⁶,
 D. Nitz⁸⁹, D. Nosek²⁶, L. Nožka²⁷, M. Nyklicek²⁷, J. Oehlschläger³⁷,
 A. Olinto⁹⁶, P. Oliva³⁶, V.M. Olmos-Gilbaja⁷⁸, M. Ortiz⁷⁵, F. Ortolani⁴⁹,
 N. Pacheco⁷⁶, D. Pakk Selmi-Dei¹⁸, M. Palatka²⁷, J. Pallotta³, G. Parente⁷⁸,
 E. Parizot³¹, S. Parlati⁵⁵, S. Pastor⁷⁴, M. Patel⁸¹, T. Paul⁹¹, V. Pavlidou^{96 c},
 K. Payet³⁴, M. Pech²⁷, J. Pękala⁶⁹, R. Pelayo⁶², I.M. Pepe²¹, L. Perrone⁴⁷,
 R. Pesce⁴⁴, E. Petermann¹⁰⁰, S. Petrera⁴⁵, P. Petrinca⁴⁹, A. Petrolini⁴⁴,
 Y. Petrov⁸⁵, J. Petrovic⁶⁷, C. Pfendner¹⁰³, R. Piegaia⁴, T. Pierog³⁷,
 M. Pimenta⁷¹, T. Pinto⁷⁴, V. Pirronello⁵⁰, O. Pisanti⁴⁸, M. Platino²,
 J. Pochon¹, V.H. Ponce¹, M. Pontz⁴², P. Privitera⁹⁶, M. Prouza²⁷, E.J. Quel³,
 J. Rautenberg³⁶, O. Ravel³⁵, D. Ravignani², A. Redondo⁷⁶, S. Reucroft⁹¹,
 B. Revenu³⁵, F.A.S. Rezende¹⁴, J. Ridky²⁷, S. Riggi⁵⁰, M. Risse³⁶,
 C. Rivière³⁴, V. Rizi⁴⁵, C. Robledo⁵⁹, G. Rodriguez⁴⁹, J. Rodriguez
 Martino⁵⁰, J. Rodriguez Rojo⁹, I. Rodriguez-Cabo⁷⁸, M.D. Rodríguez-Frías⁷⁶,
 G. Ros^{75, 76}, J. Rosado⁷⁵, T. Rossler²⁸, M. Roth³⁷, B. Rouillé-d'Orfeuil³¹,
 E. Roulet¹, A.C. Rovero⁷, F. Salamida⁴⁵, H. Salazar^{59 b}, G. Salina⁴⁹,
 F. Sánchez⁶⁴, M. Santander⁹, C.E. Santo⁷¹, E.M. Santos²³, F. Sarazin⁸⁴,
 S. Sarkar⁷⁹, R. Sato⁹, N. Scharf⁴⁰, V. Scherini³⁶, H. Schieler³⁷, P. Schiffer⁴⁰,
 A. Schmidt³⁸, F. Schmidt⁹⁶, T. Schmidt⁴¹, O. Scholten⁶⁶, H. Schoorlemmer⁶⁵,
 J. Schovancova²⁷, P. Schovánek²⁷, F. Schroeder³⁷, S. Schulte⁴⁰,

F. Schüssler³⁷, D. Schuster⁸⁴, S.J. Sciutto⁶, M. Scuderi⁵⁰, A. Segreto⁵³,
D. Semikoz³¹, M. Settimo⁴⁷, R.C. Shellard^{14, 15}, I. Sidelnik², B.B. Siffert²³,
A. Smiałkowski⁷⁰, R. Šmída²⁷, B.E. Smith⁸¹, G.R. Snow¹⁰⁰, P. Sommers⁹³,
J. Sorokin¹¹, H. Spinka^{82, 87}, R. Squartini⁹, E. Strazzeri³², A. Stutz³⁴,
F. Suarez², T. Suomijärvi³⁰, A.D. Supanitsky⁶⁴, M.S. Sutherland⁹²,
J. Swain⁹¹, Z. Szadkowski⁷⁰, A. Tamashiro⁷, A. Tamburro⁴¹, T. Tarutina⁶,
O. Taşcău³⁶, R. Tcaciuc⁴², D. Tcherniakhovski³⁸, N.T. Thao¹⁰⁵,
D. Thomas⁸⁵, R. Ticona¹³, J. Tiffenberg⁴, C. Timmermans^{67, 65},
W. Tkaczyk⁷⁰, C.J. Todero Peixoto²², B. Tomé⁷¹, A. Tonachini⁵¹, I. Torres⁵⁹,
P. Travnicek²⁷, D.B. Tridapalli¹⁷, G. Tristram³¹, E. Trovato⁵⁰, V. Tuci⁴⁹,
M. Tueros⁶, R. Ulrich³⁷, M. Unger³⁷, M. Urban³², J.F. Valdés Galicia⁶⁴,
I. Valiño³⁷, L. Valore⁴⁸, A.M. van den Berg⁶⁶, J.R. Vázquez⁷⁵,
R.A. Vázquez⁷⁸, D. Veberič^{73, 72}, A. Velarde¹³, T. Venters⁹⁶, V. Verzi⁴⁹,
M. Videla⁸, L. Villaseñor⁶³, S. Vorobiov⁷³, L. Voyvodic⁸⁷ ‡, H. Wahlberg⁶,
P. Wahrlich¹¹, O. Wainberg², D. Warner⁸⁵, A.A. Watson⁸¹, S. Westerhoff¹⁰³,
B.J. Whelan¹¹, G. Wieczorek⁷⁰, L. Wiencke⁸⁴, B. Wilczyńska⁶⁹,
H. Wilczyński⁶⁹, C. Wileman⁸¹, M.G. Winnick¹¹, H. Wu³², B. Wundheiler²,
T. Yamamoto⁹⁶ ^a, P. Younk⁸⁵, G. Yuan⁸⁸, E. Zas⁷⁸, D. Zavrtanik^{73, 72},
M. Zavrtanik^{72, 73}, I. Zaw⁹⁰, A. Zepeda⁶⁰ ^b, M. Ziolkowski⁴²

¹ Centro Atómico Bariloche and Instituto Balseiro (CNEA-
UNCuyo-CONICET), San Carlos de Bariloche, Argentina

² Centro Atómico Constituyentes (Comisión Nacional de Energía
Atómica/CONICET/UTN-FRBA), Buenos Aires, Argentina

³ Centro de Investigaciones en Láseres y Aplicaciones, CITEFA and
CONICET, Argentina

⁴ Departamento de Física, FCEyN, Universidad de Buenos Aires y
CONICET, Argentina

⁶ IFLP, Universidad Nacional de La Plata and CONICET, La Plata,
Argentina

⁷ Instituto de Astronomía y Física del Espacio (CONICET), Buenos Aires,
Argentina

⁸ Observatorio Meteorológico Parque Gral. San Martín (UTN-
FRM/CONICET/CNEA), Mendoza, Argentina

⁹ Pierre Auger Southern Observatory, Malargüe, Argentina

¹⁰ Pierre Auger Southern Observatory and Comisión Nacional de Energía
Atómica, Malargüe, Argentina

¹¹ University of Adelaide, Adelaide, S.A., Australia

¹² Universidad Católica de Bolivia, La Paz, Bolivia

¹³ Universidad Mayor de San Andrés, Bolivia

¹⁴ Centro Brasileiro de Pesquisas Físicas, Rio de Janeiro, RJ, Brazil

¹⁵ Pontifícia Universidade Católica, Rio de Janeiro, RJ, Brazil

¹⁶ Universidade de São Paulo, Instituto de Física, São Carlos, SP, Brazil

¹⁷ Universidade de São Paulo, Instituto de Física, São Paulo, SP, Brazil

¹⁸ Universidade Estadual de Campinas, IFGW, Campinas, SP, Brazil

- ¹⁹ Universidade Estadual de Feira de Santana, Brazil
- ²⁰ Universidade Estadual do Sudoeste da Bahia, Vitoria da Conquista, BA, Brazil
- ²¹ Universidade Federal da Bahia, Salvador, BA, Brazil
- ²² Universidade Federal do ABC, Santo André, SP, Brazil
- ²³ Universidade Federal do Rio de Janeiro, Instituto de Física, Rio de Janeiro, RJ, Brazil
- ²⁴ Universidade Federal Fluminense, Instituto de Fisica, Niterói, RJ, Brazil
- ²⁶ Charles University, Faculty of Mathematics and Physics, Institute of Particle and Nuclear Physics, Prague, Czech Republic
- ²⁷ Institute of Physics of the Academy of Sciences of the Czech Republic, Prague, Czech Republic
- ²⁸ Palacký University, Olomouc, Czech Republic
- ³⁰ Institut de Physique Nucléaire d'Orsay (IPNO), Université Paris 11, CNRS-IN2P3, Orsay, France
- ³¹ Laboratoire AstroParticule et Cosmologie (APC), Université Paris 7, CNRS-IN2P3, Paris, France
- ³² Laboratoire de l'Accélérateur Linéaire (LAL), Université Paris 11, CNRS-IN2P3, Orsay, France
- ³³ Laboratoire de Physique Nucléaire et de Hautes Energies (LPNHE), Universités Paris 6 et Paris 7, CNRS-IN2P3, Paris Cedex 05, France
- ³⁴ Laboratoire de Physique Subatomique et de Cosmologie (LPSC), Université Joseph Fourier, INPG, CNRS-IN2P3, Grenoble, France
- ³⁵ SUBATECH, CNRS-IN2P3, Nantes, France
- ³⁶ Bergische Universität Wuppertal, Wuppertal, Germany
- ³⁷ Forschungszentrum Karlsruhe, Institut für Kernphysik, Karlsruhe, Germany
- ³⁸ Forschungszentrum Karlsruhe, Institut für Prozessdatenverarbeitung und Elektronik, Germany
- ³⁹ Max-Planck-Institut für Radioastronomie, Bonn, Germany
- ⁴⁰ RWTH Aachen University, III. Physikalisches Institut A, Aachen, Germany
- ⁴¹ Universität Karlsruhe (TH), Institut für Experimentelle Kernphysik (IEKP), Karlsruhe, Germany
- ⁴² Universität Siegen, Siegen, Germany
- ⁴⁴ Dipartimento di Fisica dell'Università and INFN, Genova, Italy
- ⁴⁵ Università dell'Aquila and INFN, L'Aquila, Italy
- ⁴⁶ Università di Milano and Sezione INFN, Milan, Italy
- ⁴⁷ Dipartimento di Fisica dell'Università del Salento and Sezione INFN, Lecce, Italy
- ⁴⁸ Università di Napoli "Federico II" and Sezione INFN, Napoli, Italy
- ⁴⁹ Università di Roma II "Tor Vergata" and Sezione INFN, Roma, Italy
- ⁵⁰ Università di Catania and Sezione INFN, Catania, Italy
- ⁵¹ Università di Torino and Sezione INFN, Torino, Italy

- ⁵³ Istituto di Astrofisica Spaziale e Fisica Cosmica di Palermo (INAF),
Palermo, Italy
- ⁵⁴ Istituto di Fisica dello Spazio Interplanetario (INAF), Università di Torino
and Sezione INFN, Torino, Italy
- ⁵⁵ INFN, Laboratori Nazionali del Gran Sasso, Assergi (L'Aquila), Italy
- ⁵⁹ Benemérita Universidad Autónoma de Puebla, Puebla, Mexico
- ⁶⁰ Centro de Investigación y de Estudios Avanzados del IPN (CINVESTAV),
México, D.F., Mexico
- ⁶¹ Instituto Nacional de Astrofisica, Optica y Electronica, Tonantzintla,
Puebla, Mexico
- ⁶² Instituto Politécnico Nacional, México, D.F., Mexico
- ⁶³ Universidad Michoacana de San Nicolas de Hidalgo, Morelia, Michoacan,
Mexico
- ⁶⁴ Universidad Nacional Autonoma de Mexico, Mexico, D.F., Mexico
- ⁶⁵ IMAPP, Radboud University, Nijmegen, Netherlands
- ⁶⁶ Kernfysisch Versneller Instituut, University of Groningen, Groningen,
Netherlands
- ⁶⁷ NIKHEF, Amsterdam, Netherlands
- ⁶⁸ ASTRON, Dwingeloo, Netherlands
- ⁶⁹ Institute of Nuclear Physics PAN, Krakow, Poland
- ⁷⁰ University of Łódź, Łódź, Poland
- ⁷¹ LIP and Instituto Superior Técnico, Lisboa, Portugal
- ⁷² J. Stefan Institute, Ljubljana, Slovenia
- ⁷³ Laboratory for Astroparticle Physics, University of Nova Gorica, Slovenia
- ⁷⁴ Instituto de Física Corpuscular, CSIC-Universitat de València, Valencia,
Spain
- ⁷⁵ Universidad Complutense de Madrid, Madrid, Spain
- ⁷⁶ Universidad de Alcalá, Alcalá de Henares (Madrid), Spain
- ⁷⁷ Universidad de Granada & C.A.F.P.E., Granada, Spain
- ⁷⁸ Universidad de Santiago de Compostela, Spain
- ⁷⁹ Rudolf Peierls Centre for Theoretical Physics, University of Oxford,
Oxford, United Kingdom
- ⁸¹ School of Physics and Astronomy, University of Leeds, United Kingdom
- ⁸² Argonne National Laboratory, Argonne, IL, USA
- ⁸³ Case Western Reserve University, Cleveland, OH, USA
- ⁸⁴ Colorado School of Mines, Golden, CO, USA
- ⁸⁵ Colorado State University, Fort Collins, CO, USA
- ⁸⁶ Colorado State University, Pueblo, CO, USA
- ⁸⁷ Fermilab, Batavia, IL, USA
- ⁸⁸ Louisiana State University, Baton Rouge, LA, USA
- ⁸⁹ Michigan Technological University, Houghton, MI, USA
- ⁹⁰ New York University, New York, NY, USA
- ⁹¹ Northeastern University, Boston, MA, USA
- ⁹² Ohio State University, Columbus, OH, USA

- ⁹³ Pennsylvania State University, University Park, PA, USA
⁹⁴ Southern University, Baton Rouge, LA, USA
⁹⁵ University of California, Los Angeles, CA, USA
⁹⁶ University of Chicago, Enrico Fermi Institute, Chicago, IL, USA
⁹⁸ University of Hawaii, Honolulu, HI, USA
¹⁰⁰ University of Nebraska, Lincoln, NE, USA
¹⁰¹ University of New Mexico, Albuquerque, NM, USA
¹⁰² University of Pennsylvania, Philadelphia, PA, USA
¹⁰³ University of Wisconsin, Madison, WI, USA
¹⁰⁴ University of Wisconsin, Milwaukee, WI, USA
¹⁰⁵ Institute for Nuclear Science and Technology (INST), Hanoi, Vietnam
(‡) Deceased
(a) at Konan University, Kobe, Japan
(b) On leave of absence at the Instituto Nacional de Astrofisica, Optica y
Electronica
(c) at Caltech, Pasadena, USA

Abstract

Atmospheric parameters, such as pressure (P), temperature (T) and density ($\rho \propto P/T$), affect the development of extensive air showers initiated by energetic cosmic rays. We have studied the impact of atmospheric variations on extensive air showers by means of the surface detector of the Pierre Auger Observatory. The rate of events shows a $\sim 10\%$ seasonal modulation and $\sim 2\%$ diurnal one. We find that the observed behaviour is explained by a model including the effects associated with the variations of P and ρ . The former affects the longitudinal development of air showers while the latter influences the Molière radius and hence the lateral distribution of the shower particles. The model is validated with full simulations of extensive air showers using atmospheric profiles measured at the site of the Pierre Auger Observatory.

Key words: extensive air showers, UHECR, atmosphere, weather

PACS: 96.50.sd, 96.50.sb, 96.50.sf

1 Introduction

High-energy cosmic rays (CRs) are measured by recording the extensive air showers (EAS) of secondary particles they produce in the atmosphere. As the atmosphere is the medium in which the shower evolves, its state affects the lateral and longitudinal development of the shower. Pressure (P) and air density (ρ) are the properties of the atmosphere that mostly affect the EAS. An increase (or decrease) of the ground P corresponds to an increased (or

decreased) amount of matter traversed by the shower particles; this affects the stage of the longitudinal development of the shower when it reaches the ground. A decrease (or increase) of ρ increases (or decreases) the Molière radius and thus broadens (or narrows) the lateral extent of the EAS.

The properties of the primary CR, e.g., energy, mass and arrival direction, have to be inferred from EAS, which can be sampled by an array of detectors at ground level. Therefore the study and understanding of the effects of atmospheric variations on EAS in general, and on a specific detector in particular, is very important for the comprehension of the detector performances and for the correct interpretation of EAS measurements.

We have studied the atmospheric effects on EAS by means of the surface detector (SD) of the Pierre Auger Observatory, located in Malargüe, Argentina (35.2° S, 69.5° W) at 1400 m a.s.l. [1]. The Pierre Auger Observatory is designed to study CRs from $\sim 10^{18}$ eV up to the highest energies. The SD consists of 1600 water-Cherenkov detectors to detect the photons and the charged particles of the showers. It is laid out over 3000 km² on a triangular grid of 1.5 km spacing [2] and is overlooked by four fluorescence detectors (FD) [3]. The SD trigger condition, based on a 3-station coincidence [4], makes the array fully efficient above about 3×10^{18} eV. For each event, the signals in the stations are fitted to find the signal at 1000 m from the shower core, $S(1000)$, which is used to estimate the primary energy [5]. The atmosphere is continuously monitored by different meteorological stations located at the central part of the array and at each FD site. In addition, balloon-borne sensors are launched at regular intervals to measure the atmospheric temperature $T(h)$, pressure $P(h)$ and humidity $u(h)$ as a function of the altitude h above the detector [6].

In section 2, we develop a model of the expected atmospheric effects on $S(1000)$. The modulation is described by means of three coefficients that depend on the EAS zenith angle (θ). They are related to variations of P and ρ , measured at ground level, on *slower* (daily-averaged) and *faster* (within a day) time scales. The dependence of $S(1000)$ on P and ρ implies a modulation of the counting rate of events. In section 3, we study the behaviour of the recorded rate of events as a function of P and ρ . On the base of the model defined previously, we derive the P and ρ coefficients. In section 4, we perform full simulations of EAS developing in various realistic atmospheres (based on measurements from balloon soundings above the site of the Pierre Auger Observatory) in order to compare, in section 5, the results from data and simulations with the predictions of the model. We conclude in section 6.

2 Model of atmospheric effects for the surface detector of the Auger Observatory

2.1 Atmospheric effects on the measured signal

The water-Cherenkov detectors are sensitive to both the electromagnetic component and the muonic component of the EAS, which are influenced to a different extent by atmospheric effects, namely by variations of P and ρ . These in turn influence the signal measured in the detectors: for the Auger Observatory, we are in particular interested in the effects on the signal at 1000 m from the core, $S(1000)$.

The continuous measurement of atmospheric P and ρ is available only at ground level. We will show that the variation of $S(1000)$ can be fully described in terms of variation of air pressure and air density measured at the altitude of the Observatory site. If not otherwise stated, P and ρ refer to the values at ground level.

In the following, we first describe separately the effects on $S(1000)$ due to P , section 2.1.1, and ρ , section 2.1.2, and then in section 2.1.3 we provide the full parameterisation of its variations as a function of changes in P and ρ .

2.1.1 Effect of air pressure variations on the SD signal

From the point of view of P (which measures the vertical air column density above ground), an increase (decrease) corresponds to an increased (decreased) matter overburden. This implies that the shower is older (younger), i.e. in a more (less) advanced stage when it reaches the ground level.

The longitudinal profile of the electromagnetic component of the EAS is exponentially attenuated beyond the shower maximum and can be described by a Gaisser-Hillas profile [7] (see Fig. 1). We are interested in the value of the electromagnetic signal measured at 1000 m from the core, referred hereafter as S_{em} . The longitudinal development of the shower far from the core is delayed with respect to the one at the core, and can be parameterised as

$$S_{em}(E, X) \propto X^{\hat{X}_{max}/\Lambda} \exp[(\hat{X}_{max} - X)/\Lambda],$$

where E is the primary energy, X the slant depth, $\hat{X}_{max} \equiv X_{max} + \Delta$ the average maximum of the shower at 1000 m from the core with X_{max} being the shower maximum¹, $\Delta \simeq 150 \text{ g cm}^{-2}$ is the typical increase of the shower maximum at 1000 m from the core [8] and $\Lambda \simeq 100 \text{ g cm}^{-2}$ is the effective

¹ $X_{max} \simeq 750 \text{ g cm}^{-2}$ for 10^{19} eV showers according to the elongation rate mea-

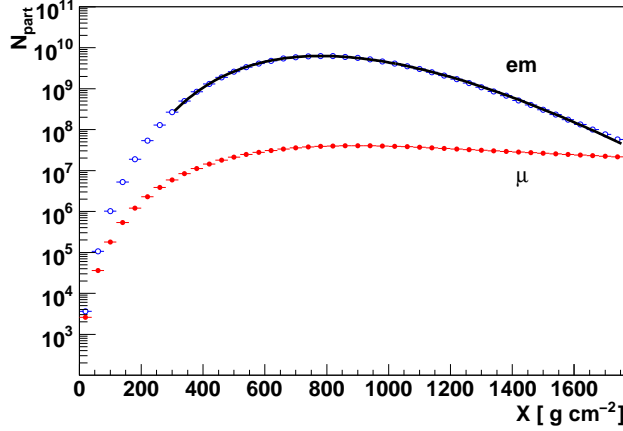


Fig. 1. Average longitudinal profile of three hundred proton-initiated showers with $E = 10^{19}$ eV, and zenith angle $\theta = 60^\circ$, simulated with CORSIKA-QGSJETII (open blue circles represent the electromagnetic component, red bullets the muonic one). The black continuous line is a fit of the electromagnetic profile with a Gaisser-Hillas function.

attenuation length after the maximum [9]. Therefore, a change in P affects S_{em} :

$$\frac{1}{S_{em}} \frac{dS_{em}}{dP} \simeq -\frac{1}{g} \left[1 - \frac{\hat{X}_{max}}{X} \right] \frac{\sec \theta}{\Lambda} \quad (1)$$

where $g \, dX = dP \sec \theta$ is used, with g the acceleration of gravity, and θ the shower zenith angle. Due to the flat longitudinal development of the muons (see Fig. 1), no significant pressure dependence is expected for the muonic component.

2.1.2 Effect of air density variations on the SD signal

Regarding ρ , this affects the Molière radius r_M

$$r_M \equiv \frac{E_s}{E_c} \frac{X_0}{\rho} \simeq \frac{91 \text{ m}}{\rho / (\text{kg m}^{-3})}$$

where $E_s \equiv m_e c^2 \sqrt{4\pi/\alpha} \simeq 21$ MeV is the energy constant characterising the energy loss due to multiple Coulomb scattering, $E_c \simeq 86$ MeV is the critical energy in air and $X_0 \simeq 37.1$ g cm $^{-2}$ is the radiation length in air. A variation in r_M affects the lateral distribution of the electromagnetic component of the EAS, which can be approximately described with a Nishimura-Kamata-Greisen (NKG) profile [11,12]. At a large distance r from the core, it behaves as $S_{em}(r) \propto N_{em}(r) \propto r_M^{-2} (r/r_M)^{-\eta}$, where $\eta \simeq 6.5 - 2s$ and $s = 3X/(X + 2X_{max})$

surement with the FD at the Pierre Auger Observatory [10]

is the age of the shower. Hence, a change in ρ affects S_{em} :

$$\frac{1}{S_{em}} \frac{dS_{em}}{d\rho} \simeq \frac{(2 - \eta)}{\rho}. \quad (2)$$

In fact, the relevant value of r_M is the one corresponding to the air density ρ^* two radiation lengths above ground [12] in the direction of the incoming shower. This corresponds to $\simeq 700 \text{ m} \cos \theta$ above the site of the Pierre Auger Observatory. On time scales of one day or more, the temperature gradient (dT/dh) in the lowest layers of the atmosphere (the planetary boundary layer, which extends up to about 1 km above ground level) can be described by an average value of $\simeq -5.5^\circ\text{C km}^{-1}$ at the site of the Auger Observatory. Therefore the variation of ρ^* on temporal scales of one day essentially follows that of ρ . An additional effect is related to the diurnal variations of dT/dh , because during the day the surface of the Earth is heated by solar radiation, producing a steeper dT/dh in the boundary layer. On the other hand, during the night the surface is cooled by the emission of long wavelength radiation: dT/dh becomes smaller and even T inversions can be observed before sunrise. As a result, the amplitude of the diurnal variation in T (and ρ) is smaller at two radiation lengths above ground than at ground level. It is then useful to separate the daily modulation from the longer term one introducing the average daily density ρ_d and the instantaneous departure from it, $\rho - \rho_d$. Therefore, the dependence of S_{em} on ρ can be modeled by

$$S_{em} = S_{em}^0 \left[1 + \alpha_\rho^{em}(\rho_d - \rho_0) + \beta_\rho^{em}(\rho - \rho_d) \right]$$

where $\rho_0 = 1.06 \text{ kg m}^{-3}$ is chosen as the reference value of ρ and is the average value measured at the site of the Pierre Auger Observatory over more than three years (1 Jan 2005 - 31 Aug 2008).

Concerning the muonic component of the signal at 1000 m from the core, S_μ , its dependence on ρ can be parameterised as

$$S_\mu = S_\mu^0 \left[1 + \alpha_\rho^\mu(\rho_d - \rho_0) \right].$$

The ρ dependence is written in terms of $\rho_d - \rho_0$ only because, as the muons are produced high in the atmosphere, their contribution to signal is not expected to depend on the daily modulations taking place in the boundary layer.

2.1.3 Model of atmospheric effects on $S(1000)$

The dependence of the total signal at 1000 m from the core, $S(1000) \equiv S = S_{em} + S_\mu$, upon P and ρ can hence be written as

$$S = S_0 \left[1 + \alpha_P(P - P_0) + \alpha_\rho(\rho_d - \rho_0) + \beta_\rho(\rho - \rho_d) \right] \quad (3)$$

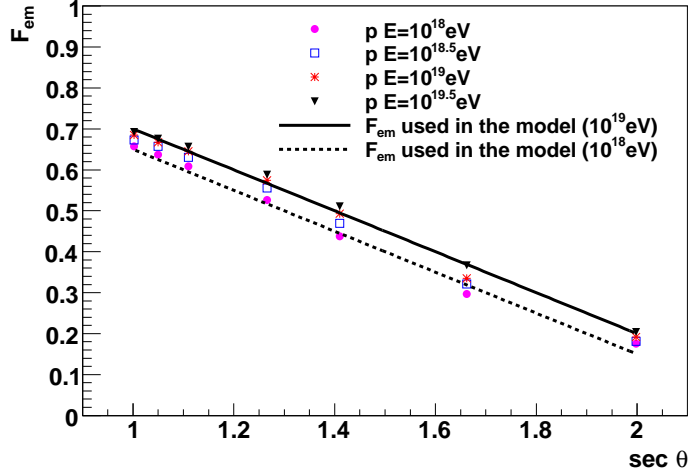


Fig. 2. Fraction of the total signal induced by the electromagnetic component of the shower at ground level at a distance of 1000 m from the shower axis (F_{em}) as a function of $\sec \theta$. A linear dependence of F_{em} on $\sec \theta$ (solid and dashed lines) is assumed in this work.

where $P_0 = 862$ hPa is the reference P at the site of the Pierre Auger Observatory, S_0 is the value of the total signal at reference pressure and density ($P = P_0$ and $\rho = \rho_d = \rho_0$), and

$$\alpha_P = F_{em} \alpha_P^{em} \quad \alpha_\rho = F_{em} \alpha_\rho^{em} + (1 - F_{em}) \alpha_\rho^\mu \quad \beta_\rho = F_{em} \beta_\rho^{em} \quad (4)$$

where $F_{em} \equiv S_{em}/S$ is the electromagnetic fraction of the signal at 1000 m from the core. The values of F_{em} are obtained by means of proton-initiated showers simulated with CORSIKA-QGSJETII (see section 4): they decrease approximately linearly with $\sec \theta$ for all the simulated primary energies (see Fig. 2).

We will adopt hereafter

$$F_{em} = F_{em}^v - 0.5(\sec \theta - 1) \quad (5)$$

where $F_{em}^v \equiv F_{em}(\theta = 0)$ varies between ≈ 0.65 at 10^{18} eV and ≈ 0.7 at 10^{19} eV. We note that since the inferred electromagnetic fraction depends on the hadronic model adopted and on the CR composition assumed, the actual value of F_{em} may be different. As shown in [9], for iron-induced showers the simulated S_μ is 40% higher than in the case of protons, while the SIBYLL model [13] predicts a muonic signal 13% lower than QGSJETII for both proton and iron primaries. The corresponding variation F_{em}^v at a primary energy of 10^{19} eV would be $\simeq -11\%$ for iron with respect to proton, and $\simeq +4\%$ for SIBYLL simulations with respect to QGSJETII.

Finally, with respect to the coefficients in eq. 4:

(i) for the pressure coefficient, we have from eq. 1

$$\alpha_P^{em} \simeq -\frac{1}{g} \left[1 - \frac{\hat{X}_{max}}{X} \right] \frac{\sec \theta}{\Lambda}$$

where $X = X_v \sec \theta$ and $X_v \simeq 880 \text{ g cm}^{-2}$ is the atmospheric depth at the site of the Pierre Auger Observatory.

(ii) From eq. 2

$$\alpha_\rho^{em} \simeq -\frac{4.5 - 2s}{\rho}$$

where $s = 3/(1 + 2 \cos \theta X_{max}/X_v)$, with $X_{max}/X_v \simeq 0.85$ for 10^{19} eV primaries. Pressure effects associated to the change in the slope of the lateral distribution function due to the X dependence of s are negligible.

(iii) The coefficient β_ρ^{em} should be smaller than α_ρ^{em} (in absolute value) reflecting the reduction in the amplitude of the $\rho - \rho_d$ variations two radiation lengths above ground level. The difference should also depend on θ . For instance, assuming an exponential decrease of the density amplitude with the height h

$$\rho(h) - \rho_d(h) = \exp \left(-a \frac{h}{700 \text{ m}} \right) [\rho(0) - \rho_d(0)]$$

would lead to

$$\beta_\rho^{em} \simeq \exp(-a \cos \theta) \alpha_\rho^{em} \quad (6)$$

where a parameterises the amplitude of the daily density variation in the lower atmosphere and is completely independent of the shower development. It characterises the scale height for the decrease of the daily thermal amplitude, which becomes $1/e$ of its ground value at a height $(700 \text{ m})/a$. The value of a is expected to be of order unity.

(iv) The coefficient α_ρ^μ is expected to be small, and will be assumed to be independent of θ , because of the relatively flat longitudinal development of the muons as shown in Fig. 1. Its value will be taken to be zero since the air shower simulations are consistent with a vanishing α_ρ^μ coefficient (see section 4).

2.2 Atmospheric effects on the event rate

The dependence of the measured signal on variations of P and ρ produces also a modulation of the rate of recorded events. The trigger probability, P_{tr} , is a well defined function of the signal [4]. As atmospheric variations correspond to signal variations, this implies that the same primary particle (in particular, with the same primary energy) will induce different signals depending on P

and ρ . This in turn affects the probability for the shower to trigger the SD array.

The effect can be quantified starting from the relation between $S(1000)$ and the energy of the primary cosmic ray. In the case of the Pierre Auger Observatory, the primary energy is reconstructed as

$$E_r \propto [S(1000)]^B,$$

where $B = 1.08 \pm 0.01(stat) \pm 0.04(sys)$ is derived from the calibration of the SD energy using the FD energy measurement [14]. Following eq. 3, the primary energy $E_0(\theta, P, \rho)$ that would have been obtained for the same shower at the reference pressure P_0 and density ρ_0 , is related to E_r as follows

$$E_0 = E_r [1 - \alpha_P(P - P_0) - \alpha_\rho(\rho_d - \rho_0) - \beta_\rho(\rho - \rho_d)]^B. \quad (7)$$

In a zenith angle bin $d\theta$, the rate R of events per unit time and unit solid angle above a given signal S_{min} can be written as

$$\frac{dR}{d\theta}(\theta, S_{min}) = \frac{dA}{d\theta}(\theta) \int_{S_{min}} dS P_{tr}(S) \frac{dJ}{dS}$$

where A is the geometrical aperture and J is the flux of cosmic rays.

Assuming that the cosmic ray spectrum is a pure power law, i.e. $dJ/dE_0 \propto E_0^{-\gamma}$, using eq. 7, and neglecting the small energy dependence of the weather coefficients, we find that

$$\begin{aligned} \frac{dJ}{dS} &\propto E_0^{-\gamma} \frac{dE_0}{dS} \\ &\propto S^{-B\gamma+B-1} [1 + B(\gamma - 1) (\alpha_P(P - P_0) + \alpha_\rho(\rho_d - \rho_0) + \beta_\rho(\rho - \rho_d))]. \end{aligned}$$

From the dependence on the atmosphere of the measured CR flux above a given signal, we derive the corresponding dependence of the rate of events. If S_{min} is the minimum required signal at 1000 m from the core to trigger the array

$$\frac{dR}{d\theta} \propto [1 + a_P(P - P_0) + a_\rho(\rho_d - \rho_0) + b_\rho(\rho - \rho_d)] \int_{S_{min}} dS P_{tr}(S) S^{-B\gamma+B-1} \quad (8)$$

with the integral on the right hand side being independent of the weather variations. The coefficients a_P , a_ρ and b_ρ are then related to the coefficients describing the modulation of the signal by $a_{\rho,P} = B(\gamma - 1)\alpha_{\rho,P}$ and $b_\rho = B(\gamma - 1)\beta_\rho$.

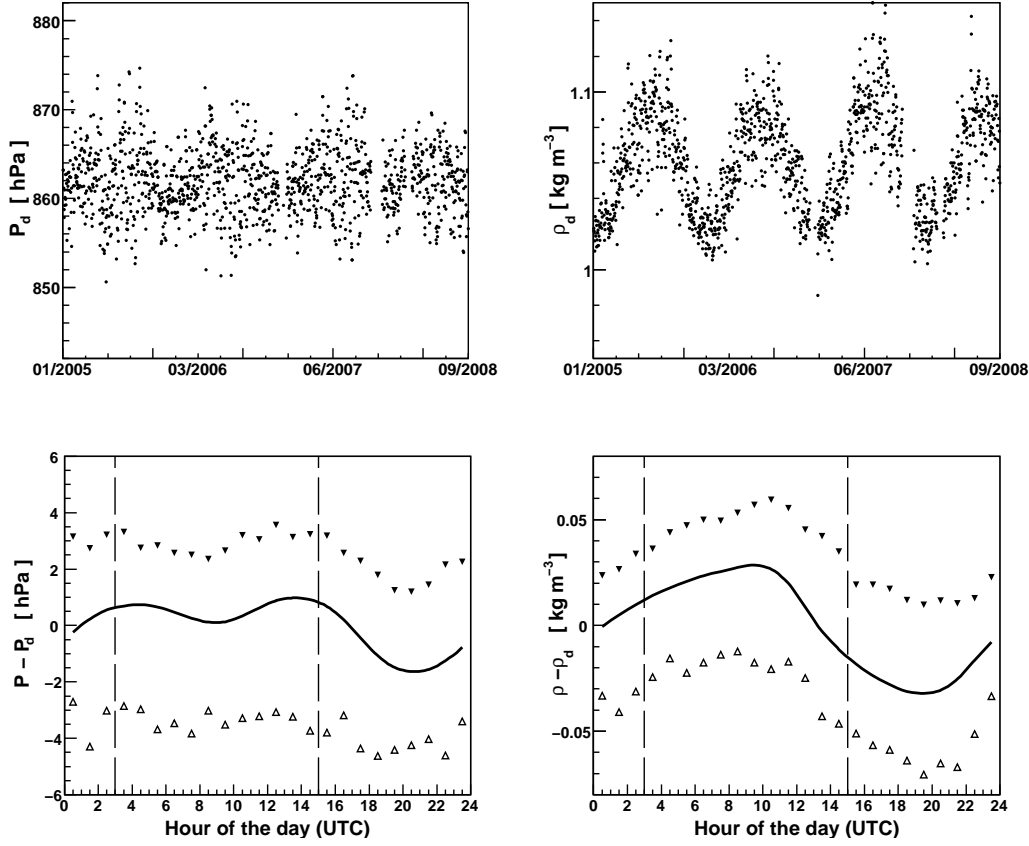


Fig. 3. Top: daily averages of P (left) and ρ (right). Bottom: diurnal variation of P (left) and ρ (right). The values are averaged over the three years considered (line), with the maximum and minimum variations marked by black and white triangles. The local time is UTC-3 h (vertical lines mark local midnight and noon).

3 Atmospheric effects on the experimental rate of events

To study the modulation of the rate of events, we use data taken by the SD from 1 January 2005 to 31 August 2008. All events with $\theta < 60^\circ$ are used, for a total of about 960 000 showers with a median energy 6×10^{17} eV. These are selected on the basis of the topology and time compatibility of the triggered detectors [4]. The station with the highest signal must be enclosed within an *active hexagon*, in which all six surrounding detectors were operational at the time of the event.

At the site of the Pierre Auger Observatory, the ground temperature and pressure are measured every five minutes. The air density is given by: $\rho = (M_m/R) (P/T)$ where M_m is the molecular mass of air, R the gas constant. The daily average density ρ_d is obtained with a smoothing procedure consisting in taking, for each time, the average value of ρ over a 24 h interval centered at

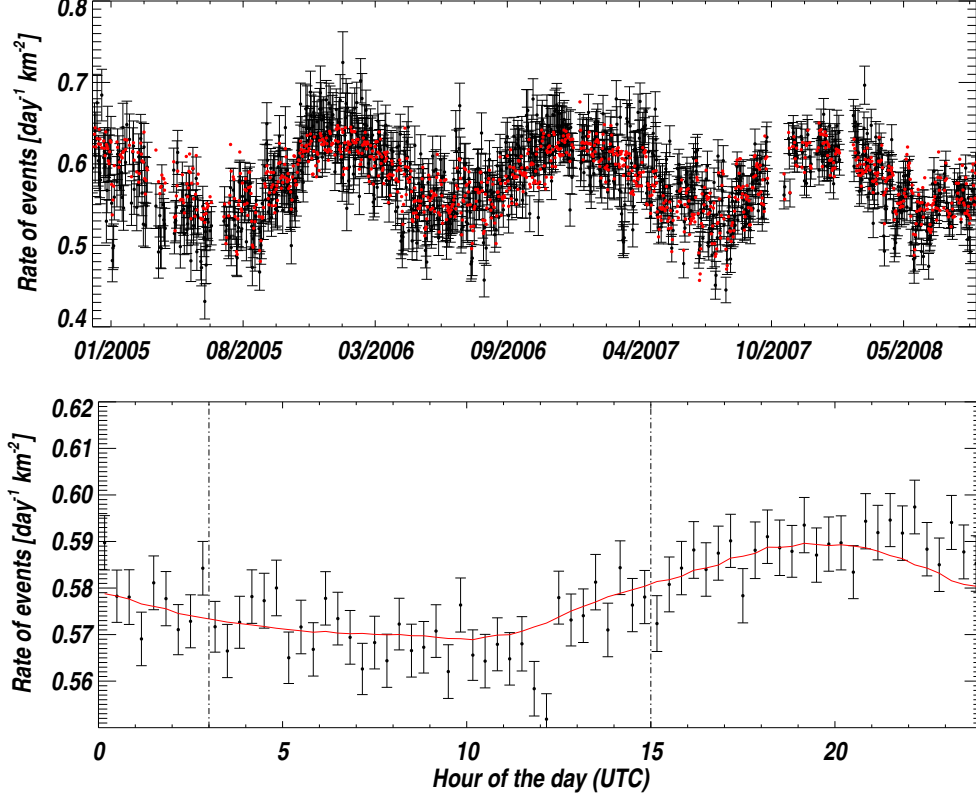


Fig. 4. Top: seasonal modulation of the measured (grey) and fitted (black points) rate of events. Bottom: diurnal modulation of the measured (grey) and fitted (black line) event rate.

the time of interest. The daily and diurnal variations of the ground P and ρ are shown in Fig. 3 (upper and lower panels respectively). The pressure exhibits less than $\pm 2\%$ variation during the period considered, while ρ_d changes up to a maximum of $\pm 8\%$ with an additional diurnal variation of density which is of $\pm 3\%$ on average with maximum values of ${}^{+6}_{-8}\%$.

In the period under study, the number of surface detectors steadily increased from about 700 to about 1590. To take this into account, rather than using the raw number of triggering events, we compute the rate every hour normalized to the sensitive area, which is calculated every second from the total area of the active hexagons. The daily and the diurnal rate of events are presented in Fig. 4 (black points), where it is evident that they both follow qualitatively the corresponding modulations of pressure and density from Fig. 3.

We use the expression given by eq. 8 to fit the measured rate of events. Assuming that the number of events n_i observed in each hour bin i follows a Poisson distribution of average μ_i , a maximum likelihood fit is performed to estimate the coefficients a_P , a_ρ and b_ρ .

The likelihood function is $L = \prod \frac{\mu_i^{n_i}}{n_i!} e^{-\mu_i}$. The expected number of events in

bin i is given by

$$\mu_i = R_0 \times A_i \times C_i$$

where R_0 is the average rate we would have observed if the atmospheric parameters were always the reference ones, i.e. $R_0 = \frac{\sum n_i}{\sum A_i C_i}$, with A_i the sensitive area in the i^{th} bin and, according to eq. 8, C_i is

$$C_i = [1 + a_P(P_i - P_0) + a_\rho(\rho_{d_i} - \rho_0) + b_\rho(\rho_i - \rho_{d_i})].$$

The fitted parameters are:

$$\begin{aligned} a_P &= (-0.0027 \pm 0.0003) \text{ hPa}^{-1} \\ a_\rho &= (-1.99 \pm 0.04) \text{ kg}^{-1} \text{ m}^3 \\ b_\rho &= (-0.53 \pm 0.05) \text{ kg}^{-1} \text{ m}^3 \end{aligned} \tag{9}$$

corresponding to a reduced χ^2 of 1.06, where $\chi^2 = \sum_i (n_i - \mu_i)^2 / \mu_i$. The result of the fit is shown in Fig. 4, compared to the daily averaged and the shorter term modulations of the measured event rate.

To check the stability of the coefficients with respect to the energy, the same study has been done for the subset of events with a reconstructed energy above 10^{18} eV, corresponding to $\simeq 20\%$ of the total statistics. The fitted coefficients are consistent within the fit uncertainties. A more detailed study of the energy dependence of the coefficients will become feasible in future with increased statistics.

4 Atmospheric effects on simulated air showers

To complete the study of atmospheric effects, we performed full EAS simulations in different atmospheric conditions. We simulated proton-initiated showers using the CORSIKA code [15] with hadronic interaction models QGSJETII [16] and Fluka [17].

We considered four fixed energies of the primary particle ($E = 10^{18}$ eV, $10^{18.5}$ eV, 10^{19} eV and $10^{19.5}$ eV) and seven fixed zenith angles between $\theta = 0^\circ$ and $\theta = 60^\circ$. For the air density profiles, we used five parameterisations (shown in Fig. 5) of the seasonal average of radio sounding campaigns carried out at the site of the Pierre Auger Observatory [6] over a wide range of variation in temperature². The set of simulations consists of 60 showers for each combination

² The atmospheric profiles are implemented in the CORSIKA code through the dependence of X on h . P , ρ and T profiles can be derived from: $\rho(h) = -dX/dh$ and $P(h) = gX(h)$. The ground values in Fig. 5 are computed at an observation

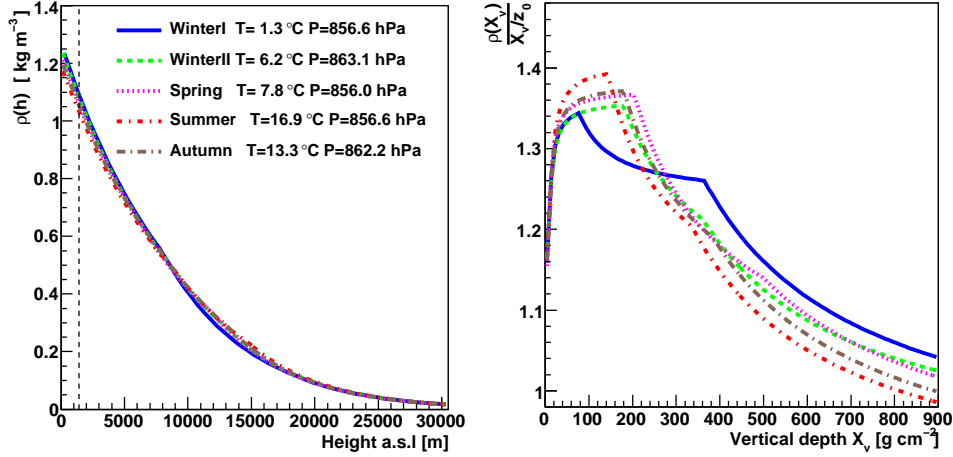


Fig. 5. Left: density profiles used in the simulations. The dashed vertical line corresponds to the altitude of the Pierre Auger Observatory (1400 m). The corresponding values of ground P and T are given in the legend. Right: same density profiles normalized to an isothermal one ($\rho(X_v) = X_v/z_0$ with $z_0 = 8.4$ km).

of atmospheric profile, energy and angle with an optimal statistical thinning level of 10^{-6} [18,19].

To compare with model predictions and data, we need to determine for each combination (E, θ) the dependence of $S(1000)$ on the variations of P and ρ . The signal can be estimated through simplified assumptions about the energy deposited by particles on the basis of their kinetic energy E_k :

- (i) e^-e^+ deposit $E_k - \epsilon_{th}$, where $\epsilon_{th} = 260$ keV is the energy threshold for Cherenkov emission in water.
- (ii) photons deposit $E_k - 2m_e - 2\epsilon_{th}$.
- (iii) muons deposit 240 MeV corresponding to the average energy released by a vertical muon crossing a 1.2 m high water-Cherenkov tank.

The contribution of each particle is multiplied by the weight assigned by the thinning algorithm. We obtain the Cherenkov signal per unit area perpendicular to the shower plane $C_{sp}(r)$. For the muons, the Cherenkov signal is proportional to the track length in the station so that: $C^\mu = C_{sp}^\mu$, whereas for the electromagnetic component: $C^{em} = \cos \theta C_{sp}^{em}$.

The left panel of Fig. 6 shows the lateral distribution $C(r) = C^{em}(r) + C^\mu(r)$, which is proportional to $S(1000)$, for four atmospheres (relative to the Spring one) in the case of $E = 10^{19}$ eV and $\theta = 18^\circ$. The effect related to the Molière radius can be clearly seen as a broadening of the lateral distribution with increasing temperature.

level $h = 1400$ m ($\simeq 880$ g cm $^{-2}$), corresponding to the altitude of the Pierre Auger Observatory.

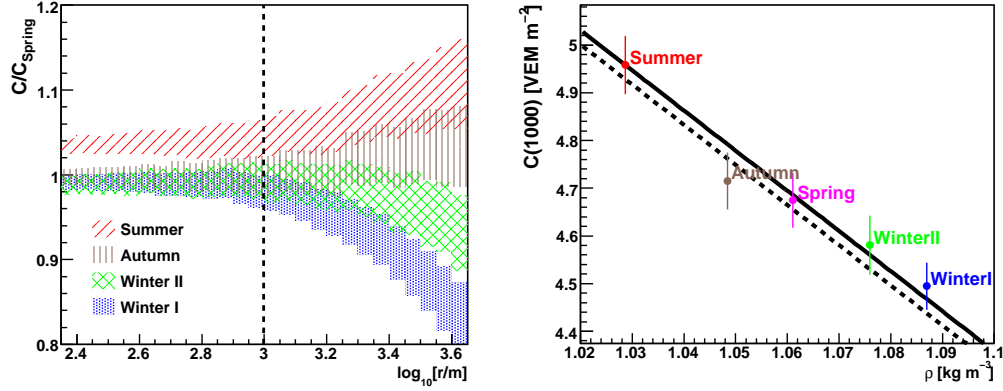


Fig. 6. Results from the proton shower simulations with $E = 10^{19}$ eV and $\theta = 18^\circ$. Left: lateral distribution of the water Cherenkov signal per unit area perpendicular to the shower axis $C(1000)$ in four atmospheres normalized to the Spring one. The uncertainty is due to shower-to-shower fluctuations. Right: $C(1000)$ as a function of ρ for the five atmospheres considered. The dashed and the continuous lines are the projections of the fit in the $(C(1000), \rho)$ plane for $P = 856$ hPa and $P = 862$ hPa, respectively.

To derive the atmospheric coefficients, we correlate the simulated $C(1000)$ (taken as the average signal between 950 m and 1050 m) with P and ρ (see eq. 3). Since we are using seasonal atmospheric profiles, we do not have access to the diurnal variation of T and thus we cannot determine the coefficient β_ρ related to the diurnal variation of ρ . The two coefficients α_ρ and α_P can be determined for each fixed energy and angle with a two dimensional fit of the $C(1000)$, obtained for the five atmospheric profiles, as function of ρ and P . As an example, we show in Fig. 6 (right) the results of the fit for the case of $E = 10^{19}$ eV and $\theta = 18^\circ$, projected on the $(C(1000), \rho)$ plane for the sake of clarity. Moreover, in the case of simulations we are able to separate the electromagnetic and the muonic contribution to the signal and thus to determine the atmospheric coefficients for each component (see Fig. 7).

5 Comparison among model, data and simulations

In this section, we compare the atmospheric coefficients derived from data with those expected from the model and simulations. We recall that with the simulations we cannot access the coefficient β_ρ , as we use average seasonal profiles for the atmosphere, while we can investigate the behaviour of separate coefficients for the electromagnetic and muonic components of EAS. On the other hand, with experimental data we cannot separate the electromagnetic and muonic components, while we can fully investigate the diurnal effects of atmospheric changes and compare measurements and expectations for all of

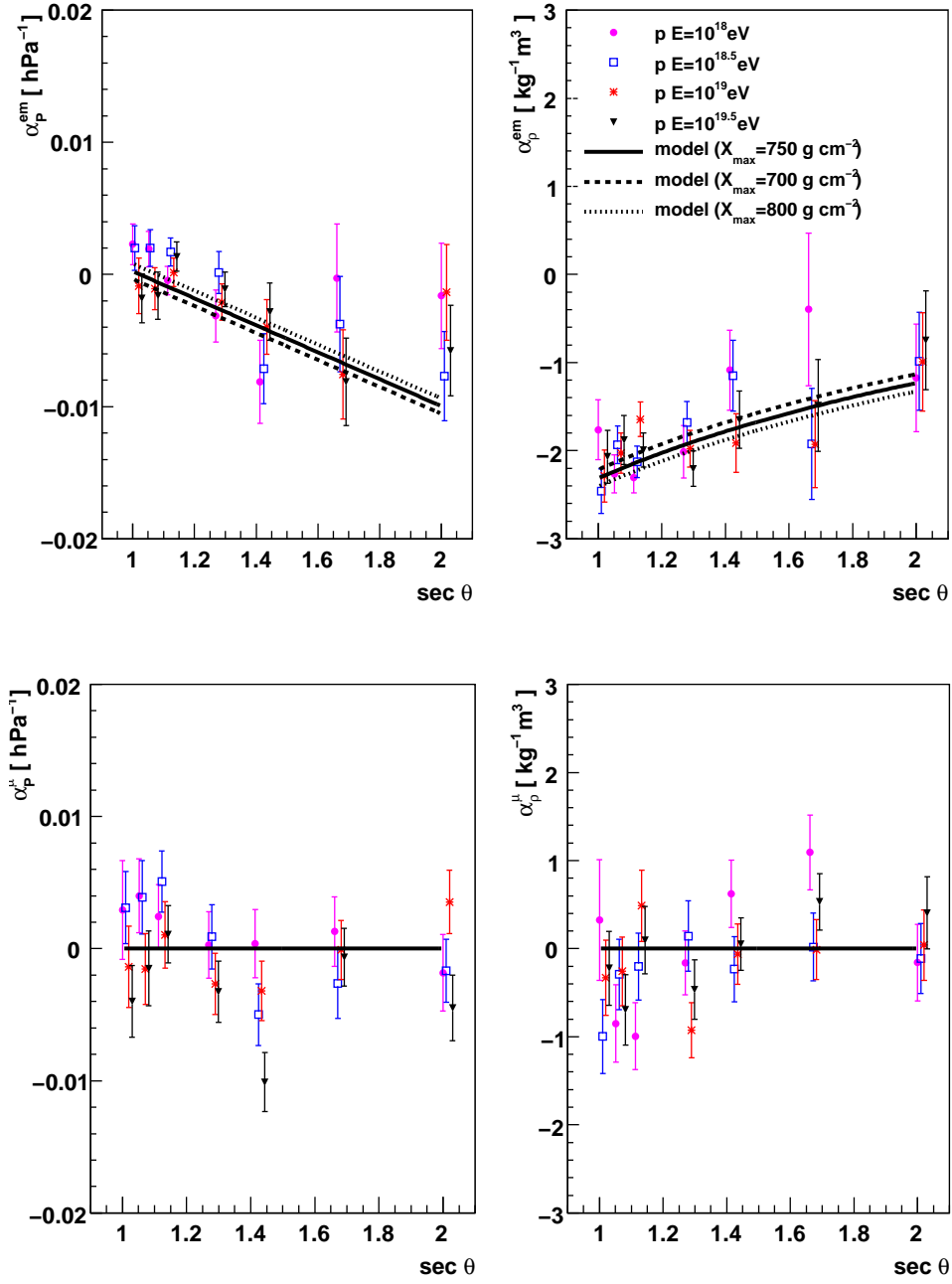


Fig. 7. Top: atmospheric coefficients (α_P on the left and α_ρ on the right) for the electromagnetic component as a function of $\sec \theta$. The differently coloured markers correspond to the four simulated energies and the lines represent the model for three different values of X_{max} . Bottom: α_P (left) and α_ρ (right) for the muonic component as a function of $\sec \theta$.

the three coefficients.

The comparison between atmospheric coefficients for the electromagnetic and muonic components of EAS from simulations and model is shown in Fig. 7, as a function of $\sec \theta$. With respect to the electromagnetic part, the model predictions for both the P and ρ coefficients, and their dependence on the shower zenith angle, are reasonable at all energies. Concerning the muonic component of the signal and its dependence on P , α_P^μ is compatible with zero at all energies, as expected from the flat longitudinal development of the number of muons. For the dependence on ρ , the model is not predictive but from the simulations we get a value of α_ρ^μ compatible with zero. This justifies the adoption in the model of vanishing coefficients for the muonic component.

The comparison of the global coefficients as a function of $\sec \theta$ is done for α_P , α_ρ and β_ρ in Figs. 8 and 9. In the case of the data, the dependence on θ has been studied by dividing the data set in subsets corresponding to five bins of equal width in $\sec \theta$. For each subset the same fitting procedure as illustrated in section 3 is used. The signal coefficients are then derived by dividing the rate coefficients by $B(\gamma - 1)$ (see the end of section 2.2). Since the bulk of the triggering events have an energy $< 10^{18}$ eV, we used $\gamma = 3.30 \pm 0.06$, as measured with the Auger Observatory below $10^{18.65}$ eV [20].

The comparison among data, simulations and model is shown for the pressure coefficient α_P and the daily component of the density coefficient α_ρ in Fig. 8 (top and bottom respectively). In the model, we use the value of X_{max} measured by the Auger Observatory at the median energy of the triggering events [10], and a F_{em}^v , corresponding at the same energy, obtained under the assumption that F_{em}^v scales linearly with the logarithm of the primary energy. The reduced χ^2 for the data-model comparison is 3.3 for α_P and 11.0 for α_ρ . For the instantaneous density coefficient β_ρ , the comparison between data and model is shown in Fig. 9. The data-model comparison gives in this case a reduced χ^2 of 0.6.

6 Conclusions

We have studied the effect of atmospheric variations (in P , T and ρ) on extensive air showers using about 960 000 events collected by the surface detector of the Pierre Auger Observatory from 1 January 2005 to 31 August 2008. We observe a significant modulation of the rate of events with the atmospheric variables, both on a seasonal scale ($\sim 10\%$) and on a shorter time scale ($\sim 2\%$ on average during a day). This modulation can be explained as due to the impact of the density and pressure changes on the shower development, which affects the energy estimator $S(1000)$, the size of the shower signal 1000 m from

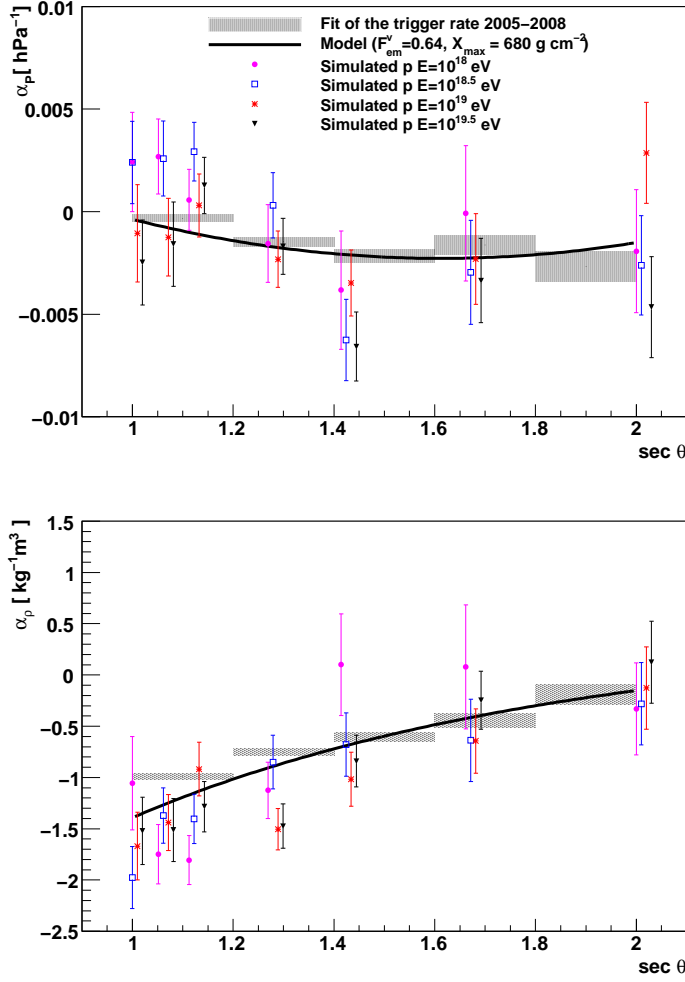


Fig. 8. Comparison of the P coefficients (top) and of the daily density coefficients (bottom) as a function of $\sec \theta$ obtained from data (grey shaded rectangle), simulations (bullets) and model (continuous line).

the shower axis. This affects the trigger probability and the rate of events above a fixed energy.

The dominant effect is due to the change with the air density of the Molière radius near ground. It induces a variation of the rate of events with associated correlation coefficients of $(-1.99 \pm 0.04) \text{ kg}^{-1}\text{m}^3$ and $(-0.53 \pm 0.05) \text{ kg}^{-1}\text{m}^3$ on long and short time scales, respectively.

The second effect is due to the pressure changes, which affect, through the variation of the amount of matter traversed, the stage of development of the showers when they reach ground. The impact of the pressure variation on the rate amounts to $(-2.7 \pm 0.3) \times 10^{-3} \text{ hPa}^{-1}$.

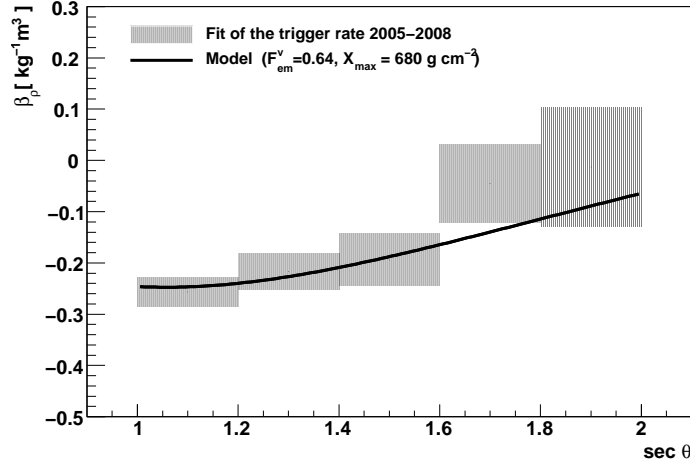


Fig. 9. Comparison of β_ρ from data with model. A fit to the data points is performed to get the value of the parameter $a = 1.7 \pm 0.1$ (see eq. 6).

Comparing the coefficients obtained from data, shower simulations in different atmospheric profiles and expectations from the model built, a good agreement is obtained, not only for the overall size of the effect but also for the zenith angle dependence.

Taking into account the atmospheric effects will allow to reduce the systematics in the energy reconstruction. Furthermore, it will be possible to correct for the seasonal modulation, which can affect the search for large scale anisotropies.

7 Acknowledgements

The successful installation and commissioning of the Pierre Auger Observatory would not have been possible without the strong commitment and effort from the technical and administrative staff in Malargüe.

We are very grateful to the following agencies and organizations for financial support: Comisión Nacional de Energía Atómica, Fundación Antorchas, Gobierno De La Provincia de Mendoza, Municipalidad de Malargüe, NDM Holdings and Valle Las Leñas, in gratitude for their continuing cooperation over land access, Argentina; the Australian Research Council; Conselho Nacional de Desenvolvimento Científico e Tecnológico (CNPq), Financiadora de Estudos e Projetos (FINEP), Fundação de Amparo à Pesquisa do Estado de Rio de Janeiro (FAPERJ), Fundação de Amparo à Pesquisa do Estado de São Paulo (FAPESP), Ministério de Ciência e Tecnologia (MCT), Brazil; AVCR AV0Z10100502 and AV0Z10100522, GAAV KJB300100801 and

KJB100100904, MSMT-CR LA08016, LC527, 1M06002, and MSM0021620859, Czech Republic; Centre de Calcul IN2P3/CNRS, Centre National de la Recherche Scientifique (CNRS), Conseil Régional Ile-de-France, Département Physique Nucléaire et Corpusculaire (PNC-IN2P3/CNRS), Département Sciences de l'Univers (SDU-INSU/CNRS), France; Bundesministerium für Bildung und Forschung (BMBF), Deutsche Forschungsgemeinschaft (DFG), Helmholtz-Gemeinschaft Deutscher Forschungszentren (HGF), Finanzministerium Baden-Württemberg, Ministerium für Wissenschaft und Forschung, Nordrhein-Westfalen, Ministerium für Wissenschaft, Forschung und Kunst, Baden-Württemberg, Germany; Istituto Nazionale di Fisica Nucleare (INFN), Ministero dell'Istruzione, dell'Università e della Ricerca (MIUR), Italy; Consejo Nacional de Ciencia y Tecnología (CONACYT), Mexico; Ministerie van Onderwijs, Cultuur en Wetenschap, Nederlandse Organisatie voor Wetenschappelijk Onderzoek (NWO), Stichting voor Fundamenteel Onderzoek der Materie (FOM), Netherlands; Ministry of Science and Higher Education, Grant Nos. 1 P03 D 014 30, N202 090 31/0623, and PAP/218/2006, Poland; Fundação para a Ciência e a Tecnologia, Portugal; Ministry for Higher Education, Science, and Technology, Slovenian Research Agency, Slovenia; Comunidad de Madrid, Consejería de Educación de la Comunidad de Castilla La Mancha, FEDER funds, Ministerio de Ciencia e Innovación, Xunta de Galicia, Spain; Science and Technology Facilities Council, United Kingdom; Department of Energy, Contract No. DE-AC02-07CH11359, National Science Foundation, Grant No. 0450696, The Grainger Foundation USA; ALFA-EC / HELEN, European Union 6th Framework Program, Grant No. MEIF-CT-2005-025057, European Union 7th Framework Program, Grant No. PIEF-GA-2008-220240, and UNESCO.

References

- [1] J. Abraham *et al.* [the Pierre Auger Collaboration], Nucl. Instrum. Meth. A **523** (2004) 50;
- [2] I. Allekotte *et al.* [the Pierre Auger Collaboration], Nucl. Instrum. Meth. A **586** (2008) 409;
- [3] J. Abraham *et al.* [the Pierre Auger Collaboration], submitted to Nucl. Instrum. Meth. A, arXiv:0907.4282;
- [4] D. Allard *et al.* [the Pierre Auger Collaboration], in Proc. 29th Int. Cosmic Ray Conf., Pune, India, **7** (2005) 287;
- [5] D. Newton *et al.*, Astropart. Phys. **26** (2007) 414;
- [6] B. Keilhauer *et al.*, Astropart. Phys. **22** (2004) 249;
J. Blümer *et al.* [the Pierre Auger Collaboration], in Proc. 29th Int. Cosmic Ray Conf., Pune, India, **7** (2005) 123;
B. Keilhauer *et al.*, Astropart. Phys. **25** (2006) 259;

- [7] T.K. Gaisser and A.M. Hillas, in Proc. 15th Int. Cosmic Ray Conf., Plovdiv, Bulgaria, **8** (1977) 353;
- [8] P. Billoir, C. Roucelle and J.C. Hamilton, astro-ph/0701583;
- [9] F. Schmidt *et al.*, Astropart. Phys. **29** (2008) 355;
- [10] M. Unger [the Pierre Auger Collaboration], in Proc. 30th Int. Cosmic Ray Conf., Merida, Mexico, **4** (2007) 373;
- [11] K. Kamata and J. Nishimura, Prog. Theor. Phys. **6** (1958) 93;
- [12] K. Greisen, Prog. in Cosmic Ray Phys. **3** (1956) 1;
- [13] J. Engel *et al.*, Phys. Rev. **D46** (1992) 5013;
R.S. Fletcher *et al.*, Phys. Rev. **D50** (1994) 5710;
R. Engel *et al.*, in Proc. 26th Int. Cosmic Ray Conf., Salt Lake City, USA, **1** (1999) 415;
- [14] J. Abraham *et al.* [the Pierre Auger Collaboration], Phys. Rev. Lett. **101** (2008) 061101;
- [15] D. Heck *et al.*, Report **FZKA 6019** (1998);
- [16] S.S. Ostapchenko, Nucl. Phys. B (Proc. Suppl.) **151** (2006), 143 and 147;
- [17] A. Fassò *et al.*, CERN-2005-10, INFN/TC_05/11, SLAC-R-773 (2005);
A. Fassò *et al.*, CHEP2003, La Jolla, USA (paper MOMT005),
arXiv:hep-ph/0306267;
- [18] A.M. Hillas, Nucl. Phys. B (Proc. Suppl.) **52** (1997) 29;
- [19] M. Koba and the Pierre Auger Collaboration, Astropart. Phys. **15** (2001) 259;
- [20] T. Yamamoto [the Pierre Auger Collaboration], in Proc. 30th Int. Cosmic Ray Conf., Merida, Mexico, **4** (2007) 335.